ROYAL SOCIETY OF CHEMISTRY

Journal Name

ARTICLE

Towards enhanced optical sensor performance: SEIRA and SERS with plasmonic nanostars

O. Bibikova,[a,b,c,d] J. Haas,[b] A.I. López-Lorente,[b] A. Popov[a e,f], M. Kinnunen,[a] I. Meglinski[a,e,f] and B. Mizaikoff[b]*

We report the preparation and characterization of plasmonic chip-based systems comprising self-assembled gold nanostars at silicon substrates that enable concomitantly enhanced Raman (surface enhanced Raman spectroscopy; SERS) and mid-infrared (surface enhanced infrared reflection or absorption spectroscopy; SEIRA) spectral signatures. The high-aspect-ratio structure of gold nanostars provides an increased number of hot spots at their surface, which results in an electric field enhancement around the nanomaterial. Gold nanostars were immobilized at a silicon substrate via a thin gold layer, and α-ω-dimercapto polyethylene glycol (SH-PEG-SH) linkers. The Raman and IR spectra of crystal violet (CV) revealed a noticeable enhancement of the analyte vibrational signal intensity in SERS and SEIRA studies resulting from the presence of the nanostars. Enhancement factors of $2.5 \cdot 10^3$ and $2.3 \cdot 10^3$ were calculated in SERS considering the CV bands at 1374.9 cm^{-1} and 1181 cm^{-1}, respectively; for SEIRA, an enhancement factor of 5.36 was achieved considering the CV band at 1585 cm^{-1}.

Introduction

During past decades plasmon-resonant nanoparticles, and especially gold nanoparticles (AuNPs) have attracted substantial interest in plasmonics, photonics, biomedical engineering, and optical sensing due to their unique ability to confine light in a nanoscopic volume.[1,2] The so called 'hot spots', i.e., regions of exceptionally high induced electric field intensities at the AuNPs or their clusters lead to strong electromagnetic field confinement, which may be enhanced in intensity by several orders of magnitude compared to the incident light.[3] Hence, the low interaction cross sections observed in Raman spectroscopy or infrared (IR) vibrational excitations may be significantly increased, thereby enabling even single molecule detection in surface enhanced Raman spectroscopy (SERS).[4,5] Within the mid-infrared (MIR) spectral range, the phenomenon of the spectral enhancement of the incident IR radiation at appropriate metal surfaces or nanostructures is called surface enhanced infrared reflection or absorption spectroscopy (SEIRAS). Enhancement of IR absorption features was first demonstrated by Hartstein et al.[6] for molecules adsorbed on nano-sized metal islands in comparison with smooth surfaces of the corresponding bulk metals.[7] Later, nanoparticles with different kinds of geometries and arrangements including linear nanorods, or nanoantennas,[8,9] split ring resonators,[10] and trapezoidal particles[11] were investigated as signal amplifiers at SEIRAS substrates.

Since IR spectroscopy is a sensitive and complementary method to Raman spectroscopy, the combination of SERS and SEIRAS provides intriguing analytical capabilities from a practical perspective, as their complementarity provides a comprehensive 'chemical fingerprint' for the identification of molecules and substrates.[12] To date, substrates capable of simultaneously enhancing Raman and IR signals were demonstrated for silver nanorod arrays,[13] gold thin-film electrodes,[14] gold nanoshell arrays[15] and multilayer structures of self-assembled gold nanospheres.[16] In the present study, this was shown for the first time using in-situ prepared gold nanostars (AuNSts).

Two mechanisms predominantly contribute to the enhancement observed both in SEIRAS and SERS, namely electromagnetic enhancement due to the high electric field strength surrounding the nanoparticles, and chemical enhancement resulting from chemical interactions between the analyte and the nanoparticles. Regarding the electromagnetic enhancement, nanoscale gaps between metal particles and the presence of sharp particle extremoties are main contributors,[17,18] as it has been demonstrated that electromagnetic fields surrounding nanostructures with sharp edges, tips or vertices are significantly more pronounced.[19-21] From that point of view, branched nanoparticles such as nanostars are geometrically ideally suited amplifiers for both Raman and IR spectroscopy because of the large number of hot

a. Optoelectronics and Measurement Techniques Laboratory, Faculty of Information Technology and Electrical Engineering, University of Oulu, Oulu 90570, Finland
b. Institute of Analytical and Bioanalytical Chemistry, Ulm University, 89081 Ulm, Germany
c. Art Photonics GmbH, 12489 Berlin, Germany
d. Research-Educational Institute of Optics and Biophotonics, Saratov National Research State University, Saratov 410012, Russian Federation
e. Interdisciplinary Laboratory of Biophotonics, Tomsk National Research State University, Tomsk 634050, Russian Federation
f. Terahertz Biomedicine Laboratory, ITMO University, St Petersburg197101, Russian Federation
*Corresponding author: Phone: +49 731 50 22750. E-mail: boris.mizaikoff@uni-um.de.

spots at their surface. Plasmon resonance (PR) of nanostars can be described via the plasmon hybridization (PH) model,[22] assuming that shorter wavelengths of the nanostars core mode allow the conduction of electrons to adiabatically follow the lower frequency of tip plasmon oscillations. This results in an antenna effect, which in turn is responsible for an increase in the absorption cross section, as well as in the respective electric field enhancement.[23] Previous studies have shown that the SERS enhancement factors of nanostars are superior to those of conventional – usually spherical – particles.[24,25] Nevertheless, to the best of our knowledge AuNSts have not been applied as signal-enhancers in IR spectroscopy to date.

Several wet-chemical methods are commonly applied for immobilizing AuNPs at different surfaces. Mid-infrared (MIR) transparent optical transducers such as silicon (Si) or gallium arsenide (GaAs)[26] have previously been functionalized using (aminopropyl) triethoxysilane (APTES)[27,28] as well as different polymers including polyethylene glycols (PEGs). In this context, self-assembled monolayers (SAMs) of α-ω-thiol functionalized PEGs represent a viable alternative towards versatile and highly stable organic immobilization architectures suitable for semiconductor surfaces.[29] Thiol groups have a high intrinsic affinity towards gold and III-V semiconductor materials, which renders thiol-PEGs a versatile tool for immobilizing AuNPs at a variety of transducer materials.[30-33]

Herein, we present a straightforward method to produce SEIRA- and SERS-active substrates based on the plasmonic properties of wet-chemically synthesized AuNSts, which were subsequently immobilized at silicon chips mediated by a gold layer and α-ω-dimercapto polyethylene glycol. Thus, obtained substrates have been characterized by microscopic and spectroscopic techniques, whereby their SERS and SEIRA properties have been demonstrated using a common analyte - crystal violet - as model substance.

Materials and Methods

Chemicals

Gold (III) chloride trihydrate (HAuCl$_4$ × 3H$_2$O), trisodium citrate dihydrate (C$_6$H$_5$O$_7$Na$_3$ ×2H$_2$O), hydrochloric acid (HCl), L(+)-ascorbic acid (AA), silver nitrate (AgNO$_3$), absolute ethanol (EtOH) were purchased from Sigma-Aldrich. Crystal violet (CV) was provided by Merck. SH-PEG-SH (MW, 2000) was purchased from Rapp Polymere GmbH (Tübingen, Germany). Milli-Q water (resistivity 18.2 MΩ cm at 25 °C; Millipore) was used in all preparations. Prior to synthesis, all glassware was washed with a mixture of nitric acid and hydrochloric acid (HNO$_3$/HCl = 1:3 mixture, Aqua Regia). Acetone and isopropyl alcohol (IPA) were purchased from Sigma-Aldrich at technical grade.

Instrumentation

Raman measurements were performed with a confocal Raman spectrometer (alpha500, Witec GmbH, Ulm, Germany). For excitation a frequency doubled Nd:YAG laser at 532 nm (second harmonic generation) was employed with the laser power of 4.32 mW measured prior the objective lens. The laser beam was

focused on the sample onto a spot of approximately 3.45 mm in diameter using a 20x/0.4 Zeiss objective.

Infrared spectroscopic studies were performed using a Vertex 70 FT-IR spectrometer (Bruker Optics, Ettlingen, Germany) equipped with a Bruker A513/QA IRRAS module equipped with a metallic line grid polarizer (KRS-5). A liquid nitrogen cooled mercury–cadmium–telluride (MCT) detector (Bruker Optics, Ettlingen, Germany) was used for signal recording. The IRRAS spectrum was collected with p-polarized radiation and an angle of incidence R=80°. Data acquisition and processing was performed using the OPUS 6.5 software package (Bruker Optics, Germany) and Essential FTIR spectroscopy toolbox (Operant LLC, USA). Scanning electron microscopy (SEM) images were acquired with a Helios Nanolab 600 scanning electron microscope (FEI, Eindhoven, The Netherlands). The Au concentration was obtained by inductively plasma coupled atomic emission spectroscopy (ICP-AES) (Ultima 2; HORIBA Jobin Yvon).

Synthesis of gold nanostars

Nanostars (NSts) were fabricated via a modified seed-mediated growth protocol following Yuan et al.[34] Seeds were prepared using the citrate reduction method introduced by France.[35] For AuNSts synthesis, 30 µL of 1M HCl and 300 mL of the seed solution were added to 10 mL of 0.25 mM HAuCl$_4$ aqueous solution at room temperature under vigorous stirring. Then, 300 µL of 2 mM AgNO$_3$ and 150 mL of 0.1 M AA were added simultaneously. The solution was stirred for 30 s while its color turned from light red to dark gray. The final gold mass concentration in the solution was 58.03 mg·L^{-1}, as calculated after ICP-AES analysis.

Functionalization of Si chips with AuNSts

Preparation of the AuNSt-functionalized silicon chips was based on diced 380 µm thick Si wafer (prime FZ, undoped) segments (1x1 cm), which were sonicated in acetone and isopropanol for 20 min, respectively. Afterwards, the substrates were dried in a nitrogen stream and cleaned in a UV/ozone chamber for 20 min removing organic residuals and to obtain a uniform oxide layer. Subsequently, 5 nm of gold layer was sputtered onto the chip surface. Thus prepared chips were immersed overnight in a 2 mM α-ω-dimercapto polyethylene glycol (SH-PEG-SH) dry and degassed ethanol solution, and subsequently rinsed with ethanol. Modified chips were then immersed overnight in an AuNSts suspension, washed by sonication in H$_2$O for 20 min, and dried under a nitrogen stream. For structured surfaces, the
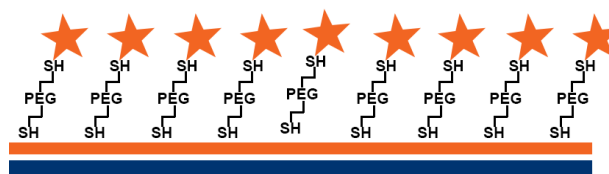

Figure 1. Scheme of the final chip structure comprising the Au layer, α-ω-dimercapto polyethylene glycol and the gold nanostars .

chips were patterned with a photoresist (TI 09 XR, MicroChemicals GmbH, Ulm, Germany) prior to the sputtering process followed by a lift-off procedure. A schematic of thus obtained layered microchips is provided in Figure 1.

Surface enhanced Raman spectroscopy studies

Raman spectra were acquired with an integration time of 1 s, averaging 10 spectra. For the measurements, 5 µL of the CV solution were drop-casted onto the SERS substrate and left to dry. Measurements were performed at different points of the sample and the average value was calculated. The intensity of the CV band at 1181 cm^{-1} was selected as an analytical signal, and subsequently used for quantification. After the measurements, the chips were cleaned with acetone, ethanol, and water for removing remaining analyte and reuse.

Surface enhanced infrared reflection absorption studies

IRRAS spectra were collected with *p*-polarized radiation at angles of incidence and detection R=80°. MIR absorbance spectra were acquired by averaging 1000 scans per spectrum in the range of 4000−500 cm^{-1} at a spectral resolution of 4 cm^{-1} vs. a gold mirror providing the background spectrum. For better comparability, a baseline correlation was performed. First, the spectra of clean chips were recorded. Then, aqueous solutions of CV were applied onto the chips by depositing 50 µL of solution at concentrations of 25, 12.5, 6.25, 3.13, and 1.56 mg·L^{-1} at the chip surface forming a thin film. Measurements were performed after evaporation of solvent. Each measurement was executed in triplicate for error calculations.

Results and discussion

Characterization of gold nanostars

The wet chemical synthesis of AuNSts has been reported in a series of publications in recent years.[35-37] The seeded growth process using 50 nm citrate spheres is among the most commonly applied strategies.[38,39] The morphology of the AuNSts was investigated with SEM and TEM. As shown in Figure 2, synthesized AuNSts with an outer diameter of approximately 90 nm have approximately 15 tips with an average length of 15 nm. These tips act as optical antennas providing for a

(a)

(b)

(c)

Figure 3. (a), (b) SEM images of a patterned Si chip comprising regions with a 5 nm Au layer, the SH-PEG-SH polymer attached on top, and immobilized AuNSts; (c) SEM image of a patterned Si chip comprising regions with a 5 nm Au layer and SH-PEG-SH, yet without immobilized AuNSts.
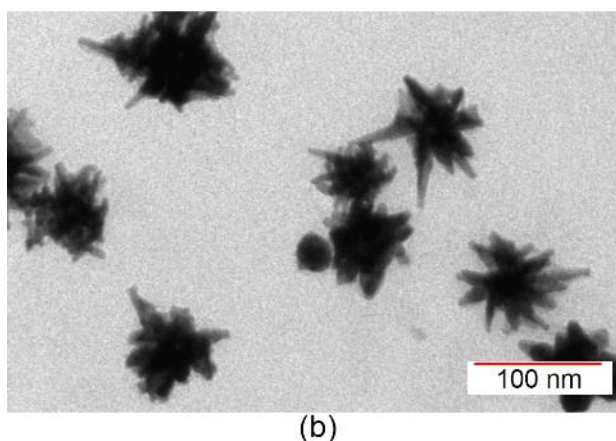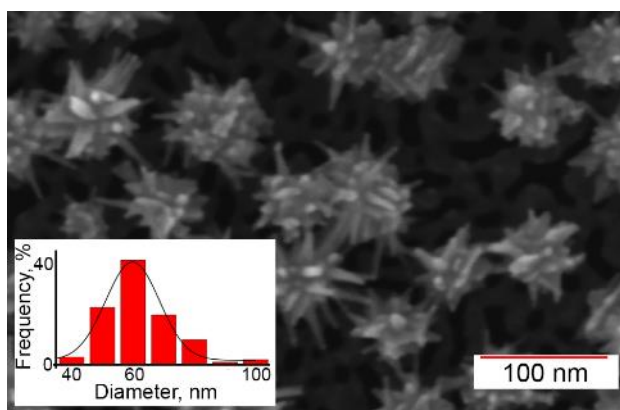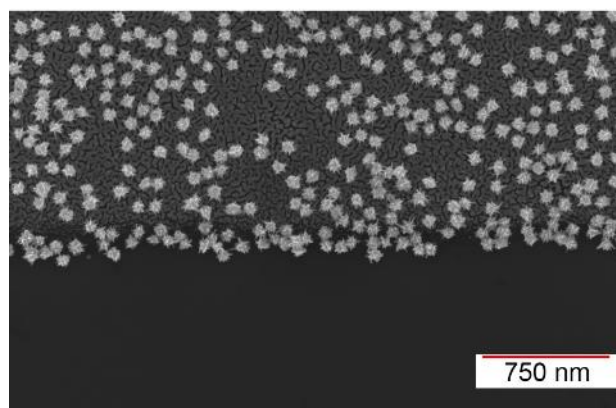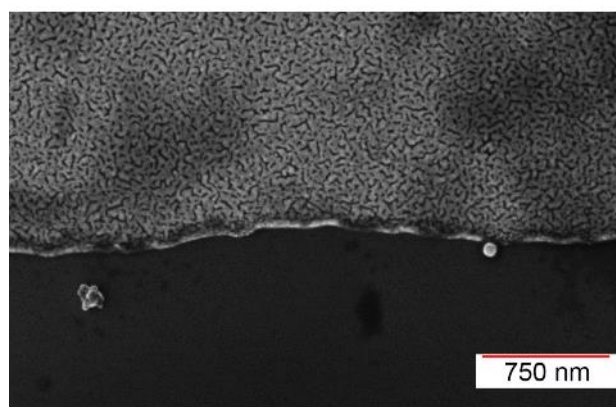
(a)

(b)

Figure 2. Typical SEM (a) and TEM (b) images of the synthesized AuNSts. The inset in Figure (a) depicts the size distribution of the AuNSts.
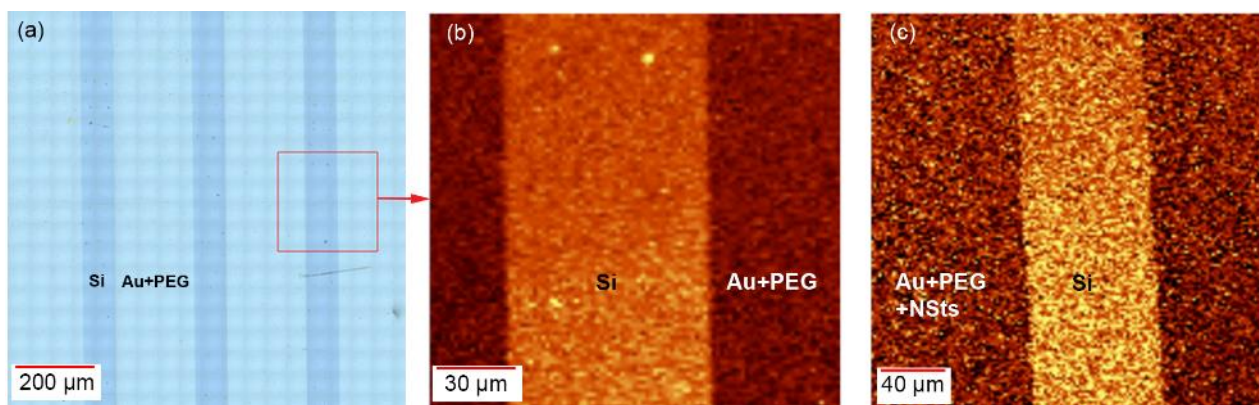
Figure 4. (a) Optical microscopy image of the structured Si chip consisting of regions with a 5 nm Au layer sputtered on top and the SH-PEG-SH polymer attached on top of it, (b) Raman image corresponding to the marked area, the intensity of Si band was selected for creating the image, (c) Raman image of a structured Si chip with a 5 nm Au layer and the SH-PEG-SH polymer and NSts attached on top.

substantial electric field enhancement upon irradiation at IR wavelengths.[40] It is well known that AuNPs are characterized by a strong plasmon resonance in the visible and NIR region, and do not inherently show a pronounced absorption in the MIR. However, the increase of the water or D_2O absorption features in presence of bare gold nanospheres was recently demonstrated, which corroborates a pronounced SEIRA effect.[41]

Characterization of functionalized silicon chips

The morphology of the SERS and SEIRAS active AuNSts substrates was investigated via SEM. As shown in Figure 3, chemically deposited AuNSts are closely packed yet remain separated, thus establishing gaps that are expected to enhance infrared signals due to the anisotropic AuNSts. A SH-PEG-SH layers were used for localized immobilization of AuNSts by sulfur-gold bonds onto the chip surface. The main advantage of chemical AuNSt deposition at the chip surface is their strong adhesion at the gold-coated silicon substrate.[42] This property significantly improves the stability of the obtained AuNSts-modified Si substrates, which allows reusability after cleaning. To prove the absence of AuNSts adsorption at the chip surface without PEG layer, photoresist patterned chips were generated such that SH-PEG-SH was found to be attached only where a gold layer had been deposited, thereby enabling further attachment of the AuNSts. The presence of well-defined locally deposited AuNSts only at PEG-covered surfaces is clearly evident in Figure 3a, b. Figure 3c shows the neat PEG layer without AuNSts. Finally, it was confirmed that cleaning procedures including washing with acetone, isopropanol, ethanol, and sonication does not affect thus immobilized AuNSt layers, as demonstrated via repeated microscopic studies (not shown).

In addition, Si chips functionalized with AuNSts were also characterized by Raman spectroscopy. For this purpose, patterned chips with strips comprising the Au-layer were prepared (Figure 4a). Subsequently, SH-PEG-SH polymer was attached only to the regions of the Si substrate where the Au-layer had been deposited, thereby enabling further attachment of AuNSts. Raman images were obtained at 150 individual points per line and 150 lines per image across a scanned area of

250 x 250 μm with an integration time of 0.1 s (Figure 4b) and 0.001 s (Figure 4c). The functionalization was evaluated via analyzing the intensity of the Si band in the Raman spectra. As evident in Figure 4, the regions where the Si surface is exposed, the intensity of the Si band is significantly higher than in areas coated with gold and the polymer (Figure 4b) and AuNSts (Figure 4c).

Surface enhanced Raman studies

The enhancing properties of AuNSts immobilized at the Si substrate were further evaluated via SERS studies. Crystal violet, a minimally fluorescent dye commonly applied for SERS studies was selected as a model analyte. The vibrational bands observed in the Raman and SERS spectra of CV can be ascribed
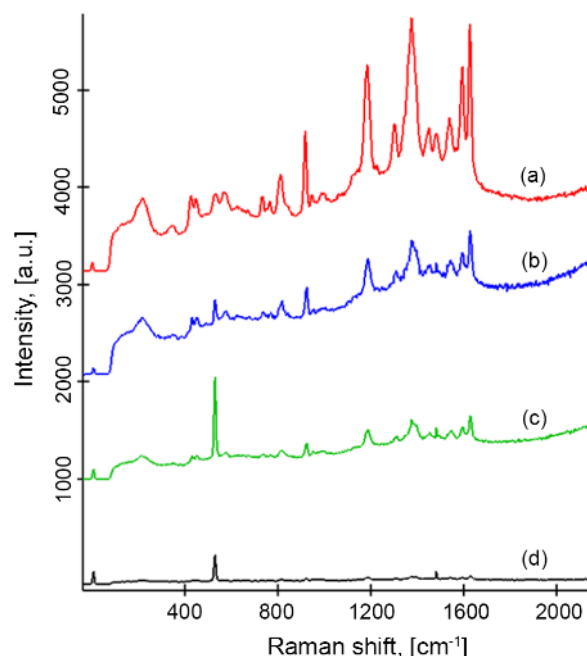

Figure 5. SERS and conventional Raman spectra of 5 μL of CV solution at different concentrations dried on bare and modified Si substrates. (a) SERS spectrum at a concentration of 12.5 mg·L^{-1} at a substrate functionalized with the AuNSts, (b) SERS spectrum of 4000 mg·L^{-1} CV on top of the gold-coated Si wafer, (c) Raman spectrum of 4000 mg·L^{-1} CV on bare Si, and (d) SERS spectrum of 100 mg·L^{-1} CV on top of the gold-coated Si substrate.

ARTICLE

Figure 7. IRRAS spectrum of CV (1.25 µg·cm^{-2}) recorded at a plasmonic chip after evaporation of the solvent.
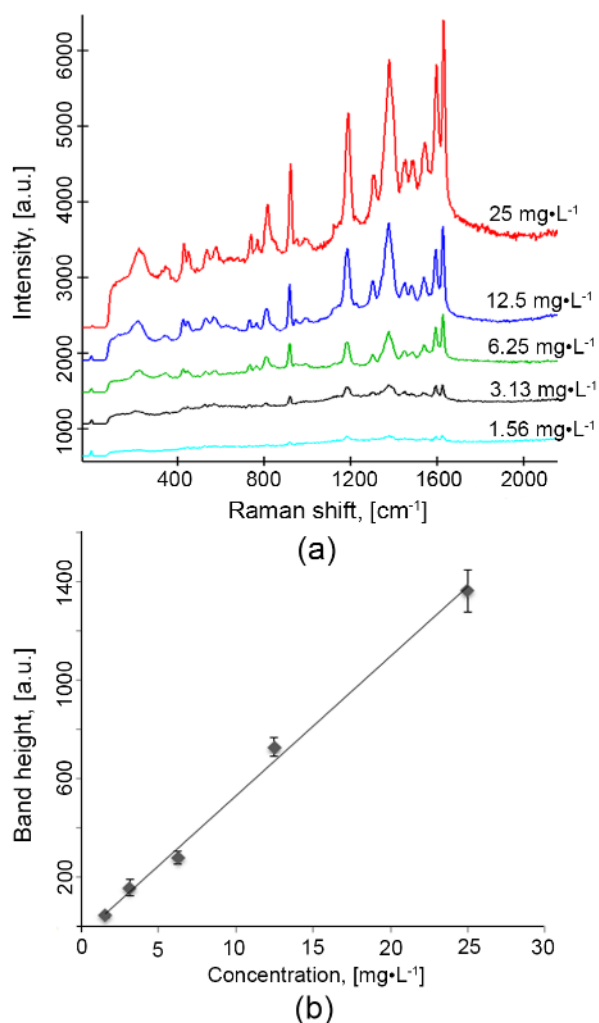
Figure 6. (a) SERS spectra of CV at different concentrations recorded at substrates functionalized with AuNSts, (b) calibration graph at different concentrations of CV evaluating the peak height of the CV band at 1181 cm^{-1}.

to the out-of-plane bending mode of C-C$_{center}$-C (416 cm^{-1}), bending mode of C-N-C, and out-of-plane aromatic C-C deformation (bands at around 517 and 554 cm^{-1}, respectively) according to literature.[43] The band at around 720 cm^{-1} results from the C-N-C symmetric stretching vibration, and the bands at 910 and 1181 cm^{-1} can be assigned to the C-H out-of-plane bending modes and C-H in-plane bending mode, respectively. The latter C-H bending mode has been selected for quantification in the present study. In addition, intense bands are also observed at 1374.9 cm^{-1} due to the stretching vibration of nitrogen and phenyl ring, and two bands around 1600 cm^{-1}, which correspond to the in-plane aromatic C-C vibrations.

Furthermore, the reusability of the SERS-active substrate was evaluated. CV was effectively removed from the functionalized chip after cleaning with water, acetone, ethanol, and finally, again water. After the cleaning procedure, no SERS signal of CV was registered, while the AuNSts remained attached to the surface of the substrate, as confirmed via repeated microscopic investigations (not shown).

For calculating the SERS enhancement factor, the Raman signal of 5 µL of 4000 mg·L^{-1} CV solution deposited at a bare Si wafer
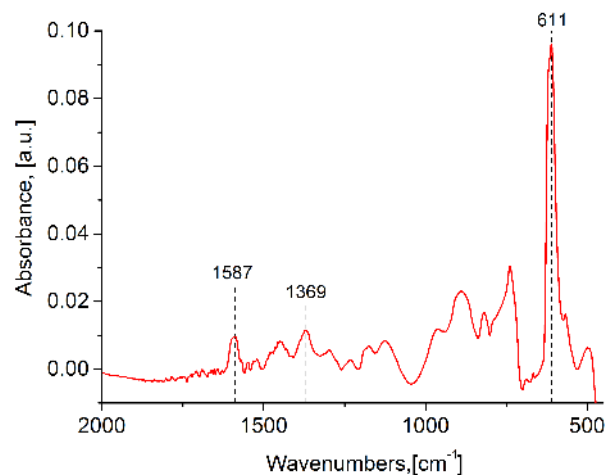
was also recorded (see Figure 5c), and compared with the enhanced signal obtained with 5 µL of 12.5 mg·L^{-1} CV solution dried at AuNSt-functionalized substrates (Figure 5a). The enhancement factor (EF) of the AuNSt-modified substrate was calculated following [44]

$$EF= (I_{SERS}/I_{Raman}) \times (N_{Raman}/N_{SERS}),$$

where I is the intensity (i.e., peak height) of the considered CV band, and N represents the total number of analyte molecules deposited on the substrate. Thus, an enhancement factor of 2.5·10^3 was calculated considering the CV band at 1374.9 cm^{-1}, whereas using the band at 1181 cm^{-1} the enhancement factor was 2.3·10^3.

For further corroborating that the observed enhancement is originated from the presence of AuNSts, similar measurements at a Si substrate only coaetd with the gold layer were performed. Figure 5 (curves b, d) depicts the Raman spectra acquired at such substrates. Comparing spectra b and c in Figure 5, a minute enhancement is observed for the 4000 mg·L^{-1} CV solution deposited at the gold-covered Si vs. the bare Si substrate. Yet, applying a solution with a concentration of 100 mg·L^{-1} at this substrate (curve d), the bands of CV are barely evident vs. the AuNSt-coated substrate (curve a).

Furthermore, the quantitative analytical performance of the developed SERS substrates was evaluated. Hence, CV solutions at different concentrations were analyzed via deposition and drying of 5 µL solution aliquots at the surface of Si-Au-PEG-AuNSt chips. Figure 6a exemplarily shows spectra obtained at different CV concentrations along with a calibration function plotting the Raman intensity of the CV band at 1181 cm^{-1} vs. the concentration (Figure 6b). Each concentration level was analyzed in triplicate with the error bars representing the standard deviation of the mean value. A straight line fit function between 1.56 and 25 mg·L^{-1} CV enabled a R^2 value of 0.995. The detection and quantification limits calculated as three- and ten-times the noise were determined at 1.51 and 5.02 mg·L^{-1}, respectively. The reproducibility expressed as the relative standard deviation (RSD) was 6.36% for a CV concentration of 25 mg·L^{-1}.
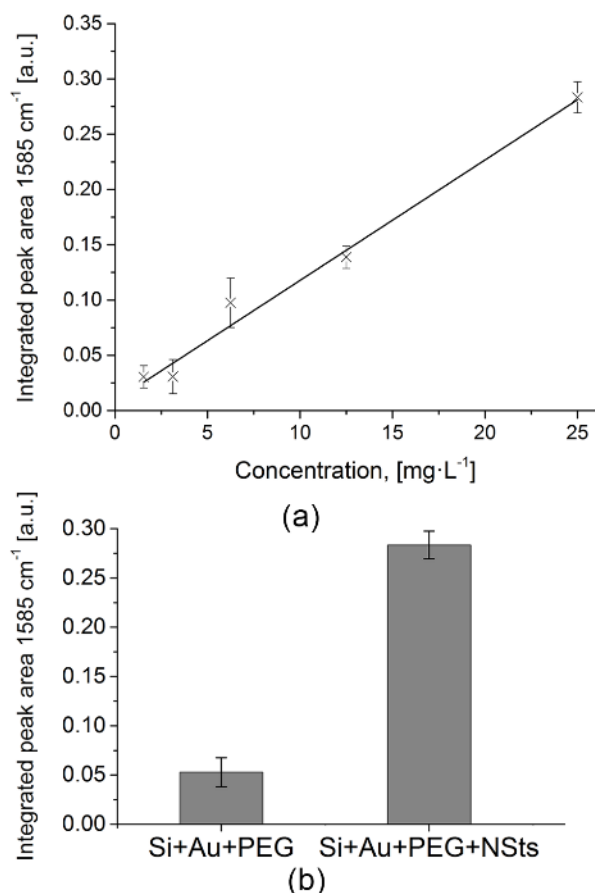
Figure 8. (a) Calibration function based on a concentration series of CV dissolved in water via peak height analysis in the IRRAS spectrum of CV at 1585 cm^{-1}. (b). CV band height at 1585 cm^{-1} after evaporation yielding a surface coverage of 1.25 µg·cm^{-2} at Si-Au-PEG-AuNSt surface in comparison to Si-Au-PEG chip surfaces.

Surface enhanced infrared reflection absorption studies

To investigate SEIRA effects at the same plasmonic chips, 50 µL of aqueous CV solutions at different concentrations (i.e., 25, 12.5, 6.25, 3.13, and 1.56 mg·L^{-1}) were drop-casted on the Si-Au-PEG-AuNSt chips. IRRAS spectra were recorded after evaporation of the solvent. Each concentration level was analyzed in triplicate with the error bars representing the standard deviation of the mean value. Figure 7 shows an exemplary spectrum of CV (25 mg·L^{-1}) recorded at a Si-Au-PEG-AuNSt chip. The most pronounced band at 611 cm^{-1} is associated with the backbone vibration of CH_2 of the PEG linker molecule. The peak at 1585 cm^{-1} was assigned to the ring stretching mode arising from the three benzene rings of the CV molecule.[45,46] Moreover, the peak at 1481 cm^{-1} was assigned to the CH_3 in-plane mode, whereas the peak at 1369 cm^{-1} was associated with the C-N vibration.[47]

A calibration function was established by plotting the intensity (i.e., peak height) of the band at 1585 cm^{-1} vs. the CV concentration (Figure 8a). The limit of detection was determined at 4 mg·L^{-1}, while the limit of quantification yielded a value of 6.67 mg·L^{-1}. The reproducibility expressed as relative standard deviation (RSD) was 2.94% at a CV concentration of 25 mg·L^{-1}.

For confirming the SEIRA effect of AuNSts, the intensity of the IR signal obtained from dried CV at a concentration of 1.25 µg·cm^{-2} after drying at a Si-Au-PEG-AuNSt chip was compared to the same concentration recorded at a Si-Au-PEG chip without AuNSts. As evident in Figure 8b, the intensity of the band is approximately 5-times higher for Si-Au-PEG-AuNSt chips. Hence, improved limits of detection via SEIRA effects enable the detection of minute analyte quantities essential, e.g., for the detection of biologically or medically relevant analytes via IR-based sensing schemes.

Table 1 summarizes the analytical features obtained for both SERS and SEIRAS studies using crystal violet as exemplary analyte and plasmonic chips based on in-situ generated immobilized gold nanostars. The limits of detection are similar for both techniques, i.e., 1.51 mg·L^{-1} for SERS and 4 mg·L^{-1} for SEIRAS. As expected, the enhancement factor achieved for SERS experiments (factor of 2.5·10^3) is much more pronounced compared to the SEIRA studies (factor of 5). Typically, enhancements reported in literature in SEIRA experiments range from a factor of 4 up to 1000,[48] whereas enhancement factors up to 10^{12}-10^{14} have been reported for SERS.[49] Nonetheless, it was demonstrated that the overall sensitivity of IR and Raman studies at such substrates is on the same order of magnitude, which renders the developed plasmonic chips utilizing gold nanostars useful substrates for complimentary vibrational spectroscopic studies.

Table 1. Figures-of-merit for SERS and SEIRA studies at plasmonic AuNSt chips for the quantitative determination of crystal violet.

	SERS	IRRAS-SEIRA
Linear range	1.56-25 mg·L^{-1}	1.56-25 mg·L^{-1}
LOD	1.51 mg·L^{-1}	4 mg·L^{-1}
LOQ	2.52 mg·L^{-1}	6.67 mg·L^{-1}
EF	2.5 · 10^3	5
RSD (%)	6.36	2.94
Sample volume (µL)	5	50

Conclusions

This study reports the development of plasmonic Si chips based on immobilized gold nanostars via in-situ chemical deposition strategies, which enable complementary surface enhanced Raman – SERS - and surface enhanced infrared – SEIRA - studies at the same substrate. The robustness of the substrate architecture readily enables applications of such signal-enhancing optical transducers in a wide variety of biochemically and biomedically relevant application scenarios such as label-free bioassays based on vibrational spectroscopies. Furthermore, the developed in-situ generation and immobilization procedures for AuNSts are also applicable for sulfur-III-V-semiconductor coupling, i.e., materials including gallium arsenide (GaAs), which have recently been demonstrated as next-generation on-chip IR evanescent field waveguides.[50-55]

Acknowledgements

Notes and references

1   R. Cao-Milán, L.M. Liz-Marzán, *Expert Opinion on Drug Delivery*, 2014, **11**, 741-752.

2   H. Jans, Q. Huo, *Chem. Soc. Rev.* **41**, 2012, 2849-2866.

3   J. Haes , S. Zou , G. C. Schatz, R. P. Van Duyne, *J. Phys. Chem.* B, 2004, **108**, 6961–6968.

4   C D'Andrea, J Bochterle, A. Toma, C. Huck, F. Neubrech, E. Messina, B. Fazio, O. M. Maragò, E. Di Fabrizio, M. Lamy de La Chapelle, P. G. Gucciardi, A. Pucci, ACS Nano, 7, 2013,3522–3531.

5   J. Vogt, C. Huck, F. Neubrech, A. Toma, D. Gerbert, A. Pucci, Phys. Chem. 2015, 17, 21169–21175.

6   A. Hartstein, J. R. Kirtley, J. R. Tsang, Phys. Rev. Lett., 1980, 45, 201–204.

7   R. Kellner, B. Mizaikoff, M. Jakusch, H. D. Wanzenboè, N. Weissenbacher, *Appl. Spectrosc*. 1997, **51**, 495-503.

8   F. Neubrech, A. Pucci, T. W. Cornelius, S. Karim, A. Garcá-Etxarri, J. Aizpurua, *Phys. Rev. Lett.* 2008, **101**,157403.

9   C. Huck, F. Neubrech, J. Vogt, A. Toma, D. Gerbert, J. Katzmann, T. Härtling, A. Pucci, *ACS Nano,* 2014, **8**, 4908–4914.

10 T. Shimada, H. Nakashima, Y. Kumagai, Y. Ishigo, M. Tsushima, A. Ikari, Y. Suzuki *J. Phys. Chem. C,* 2016, **120,** 534–541.

11 H. Aouani, H. Šípová, M. Rahmani, M. Navarro-Cia, K. Hegnerová, J. Homola, M. Hong, S. A. Maier, *ACS Nano*, 2013, **7**, 669–675.

12 S. K. Gray, *Plasmonics,* 2007, **2**, 143–146.

13 C. L. Leverette, S. A. Jacobs, S. Shanmukh, S. B. Chaney, R. A. Dluhy, Y. P. Zhao, *Appl. Spectrosc.* 2006, **60**, 906–913.

14 J. M. Delgado, J. M. Orts, J. M. Perez, A. Rodes, *J. Electroanal. Chem.* 2008, **617**, 130–140.

15 H. Wang, J. Kundu, N. J. Halas, *Angew. Chem.* 2007, **119**, 9198–9202.

16 M. Baia, F. Toderas,L. Baia,D. Maniu, S. Astilean, *Chem. Phys. Chem.* 2009, **10**, 1106 – 1111.

17 C. L. Haynes, A. D. McFarland, R. P. Van Duyne, *Anal. Chem.*, 2005, **77**, 338A–346A.

18 F. Le, D. W. Brandl, Y. A. Urzhumov, H. Wang, Kundu, J. Halas, N. J. Aizpurua, J. Nordlander, *ACS Nano*, 2008, **2**, 707–718.

19 E. C. Le Ru, J. Grand, I. Sow, W. R. C. Somerville, P. G. Etchegoin, M. Treguer-Delapierre, G. Charron, N. Felidj, G. Le´vi, J. A. Aubard, *Nano Lett.,* 2011, **11**, 5013– 5019.

20 H. Xu, E. J. Bjerneld, M. Kall, L. Börjesson, *Phys. Rev. Lett.* 1999, **83**, 4357–4360.

21 H. Xu, J. Aizpurua, M. Kall, P. Apell, *Phys. Rev. E: Stat. Phys., Plasmas, Fluids, Relat. Interdiscip. Top.* 2000, **62**, 4318–4324.

22 E. Prodan, C. Radloff, N. J. Halas, P. Nordlander, *Scienc*e, 2003, **302**,419–422.

23 G. Chirico, M. Borzenkov, P. Pallavicini, SpringerBriefs in Materials, ISBN 978-3-319-20767-4 ISBN 978-3-319-20768-1 (eBook)

24 M. Li, S. K. Cushing, J. Zhang, J .Lankford, Z. P. Aguilar, D. Ma, N. Wu, *Nanotechnology*, 2012, **23**, 115501.

25 H. Yuan, A. M. Fales, C. G. Khoury, J. Liu, T. Vo-Dinh, *J. Raman Spectrosc.,* 2013, **44**, 234–239.

26 L. Leidner, M. Ewalda, M. Siegerb, B. Mizaikof, G.Gauglitz, R. A. Lieberman, *Proc. of SPIE,* 2013, **8774**, 87740S.

27 O. Seitz, M. M. Chehimi, E. Cabet-Deliry, S. Truong, N. Felidj, C. Perruchot, S.J. Greaves, J. F. Watts, *Colloids Surface A: Physiochem. Eng. Aspects*, 2003, **218.**

28 D. Enders, T. Nagao, A. Pucci, T. Nakayama, *Surf. Sci.* 2006, **600**, L71.

29 W. Wang, Q. Q. Wei, J. Wang, B. C. Wang, S. H. Zhang, Z. Yuan, *J. Colloid Interface Sci.*, 2013, **404**, 223–229.

30 M. Tkachev, T. Anand-Kumar, A. Bitler, R. Guliamov, R. Naaman, *Engineering*, 2013, **5**, 1–12.

31 C. Kirchner, M. George, B. Stein, W. Parak, H. Gaub, M. Seitz, *Bayreuth Polym. Symp. Int. Symp. Funct. Struct. Polym. Mater.*, 2001, **4**, 266–276.

32 E. Petryaeva U. J. Krull, *Langmuir*, 2012, **28**, 13943–13951.

33 L. Leidner, M. Ewald, M. Sieger, B. Mizaikof, *Proc. SPIE*, 2013, **8774**, 1–15.

34 H. Yuan, C. G. Khoury, H. Hwang, Ch. M. Wilson, G. A. Grant, T. Vo-Dinh, *Nanotechnology,* 2012, 23, 075102.

35 M. M. Vega, A. Bonifacio, V. Lughi, S. Marsi, S. Carrato, V. Sergo, *J. Nanoparticle Res.*, 2014, **16**, 2729.

36 O. Bibikova, A. Popov, A. Bykov, A. Fales, H. Yuan, I. Skovorodkin, M. Kinnunen, S. Vainio, T. Vo-Dinh, V. Tuchin, I. Meglinski, *IEEE J. Sel. Top. Quantum Electron*. 2016, **22**, 1-8.

37 A. Guerrero-Martínez, S. Barbosa, I. Pastoriza-Santos, L.M. Liz-Marzán, *Curr. Op. Colloid Interface Sci*. 2011, **16,** 118-127.

38 O. Bibikova, A. Popov, A. Bykov, A. Prilepskyii, M. Kinnunen, K. Kordas, V. Bogatyrev, N. Khlebtsov, S. Vainio, V. Tuchin, *J. Biomed. Opt.* 2015, **20**, 076017.

39 G. Frens*, Colloid & Polymer Science*, **1972**, 250, 736–741.

40 F. Hao, C. L. Nehl, J. H. Hafner, and P. Nordlander, *Nano Lett.*, 2007, **7**, 729–732.

41 Á. I. López-Lorente, M. Sieger, M. Valcárcel, B. Mizaikof, *Anal. Chem.*, 2014, **86**, 783–789.

42 Y. Xue, X. Li, H. Li, W. Zhang, *Nat. Commun.*, 2014, **5**, 4348.

43 W.W. Yu, I.M. White, *Analyst,* 2012, **137**, 1168–1173.

44 K. Lai, Y. Zhang, R. Du, F. Zhai, B.A. Rasco, Y. Huang, *Sens. Instrumn. Food Qual*., 2011, **5**, 19.

45 W. J. Bae, K. H. Kim, Y. H. Park, W. H. Jo, *Chem. Commun*. 2003, 2768.

46 L. Li, M. Mizuhata, A. Kajinami, S. Deki, Synth. Met., 2004, 146, 17.

47 H. Kato, S. Takemura, Y. Watanabe, T. Nara, T. Hayashi, T. Sugiyama, T. Hiramatsu, N. Nanba, O. Nishikawa, and M. Taniguchi, J. Vac. Sci. Tech. A, 2007, 25, 1547.

48 M. Osawa, Top. Appl. Phys., 2001, 81, 163.

49 H.M. Lee, S.M. Jin, H.M. Kim, Y.D. Suh, Phys. Chem. Chem. Phys., 2013, 15, 5276.

50 X. Wang, M. Sieger and B. Mizaikof, *Proc. SPIE*, 2013, **8631**, 86312M–1–11.

51 L. Leidner, M. Ewald, M. Sieger and B. Mizaikof, *Proc. SPIE*, 2013, **8774**, 1–15.

52 J. Haas, R. Stach, M. Sieger, Z. Gashi, M. Godejohann and B. Mizaikof, *Anal. Methods*, 2016, **8**, 6602-6606.

53 M. Sieger, D. McMullin, T. Oener, G. Kos, M. Godejohann, R. Krska, B. Mizaikoff, *in The World Mycotoxin Forum, 8th Conference*, 2013, 314018.

54 B. Mizaikoff, X. Wang, M. Sieger, L. Faraone, J. Antoszewski, W. Lei, M. Jetter and P. Michler, 2014 Conf. Optoelectron. Microelectron. Mater. Devices, COMMAD 2014, 301–302.

55 X. Wang, S.-S. Kim, R. Rossbach, M. Jetter, P. Michler and B. Mizaikoff, *Analyst*, 2012, **137**, 2322–2327.